energies

MDPI

Article

Transition from Electromechanical Dynamics to Quasi-Electromechanical Dynamics Caused by Participation of Full Converter-Based Wind Power Generation

Jianqiang Luo [1,2], Siqi Bu [1,2,*] and Jiebei Zhu [3]

1 Shenzhen Research Institute, The Hong Kong Polytechnic University, Shenzhen 518057, China; jq.luo@connect.polyu.hk
2 Department of Electrical Engineering, The Hong Kong Polytechnic University, Kowloon, Hong Kong, China
3 School of Electrical Automation and Information Engineering, Tianjin University, Tianjin 300072, China; zhujiebei@hotmail.com
* Correspondence: siqi.bu@polyu.edu.hk

Received: 30 September 2020; Accepted: 23 November 2020; Published: 27 November 2020

check for updates

Abstract: Previous studies generally consider that the full converter-based wind power generation (FCWG) is a "decoupled" power source from the grid, which hardly participates in electromechanical oscillations. However, it was found recently that strong interaction could be induced which might incur severe resonance incidents in the electromechanical dynamic timescale. In this paper, the participation of FCWG in electromechanical dynamics is extensively investigated, and particularly, an unusual transition of the electromechanical oscillation mode (EOM) is uncovered for the first time. The detailed mathematical models of the open-loop and closed-loop power systems are firstly established, and modal analysis is employed to quantify the FCWG participation in electromechanical dynamics, with two new mode identification criteria, i.e., FCWG dynamics correlation ratio (FDCR) and quasi-electromechanical loop correlation ratio (QELCR). On this basis, the impact of different wind penetration levels and controller parameter settings on the participation of FCWG is investigated. It is revealed that if an FCWG oscillation mode (FOM) has a similar oscillation frequency to the system EOMs, there is a high possibility to induce strong interactions between FCWG dynamics and system electromechanical dynamics of the external power systems. In this circumstance, an interesting phenomenon may occur that an EOM may be dominated by FCWG dynamics, and hence is transformed into a quasi-EOM, which actively involves the participation of FCWG quasi-electromechanical state variables.

Keywords: electromechanical dynamics; FCWG dynamics; strong interaction; electromechanical loop correlation ratio (ELCR); FCWG dynamic correlation ratio (FDCR); quasi- electromechanical loop correlation ratio (QELCR)

1. Introduction

The high penetration of renewables and power electronic domination are two important aspects of the future power system [1,2]. Converter interfaced generations (CIGs) such as wind power and photovoltaic (PV) generation have been increasingly integrated into the power system at an incredible scale and speed and play a pivotal role in rendering the power system more sustainable [3–5]. As one of the promising CIGs, full converter-based wind power generation (FCWG, e.g., permanent magnet synchronous generator (PMSG)), in which two full scale converters are employed to transfer wind power to the power system, has become prevalent in the wind market due to its concise physical structure and mature control techniques [6–9]. The ever-increasing share of wind generation and its replacement of conventional synchronous generators (SGs) involve profound challenges on the electromechanical dynamics and potential threats on the oscillatory stability of the power system [10–13]. Unlike conventional rotational power sources, the integration of FCWG may introduce complex interactions with the electromechanical dynamics, which is well worth investigating, whereas it has not been thoroughly studied.

Currently, many efforts have been endeavored as to how to utilize wind generation and employ various additional controllers to mitigate electromechanical oscillations. Despite the inertia-less characteristic under the maximum power point tracking (MPPT) control strategy, by emulating an inertia response, a double fed inductor generator (DFIG) is capable of damping electromechanical oscillations [14]. Both drivetrain torsional oscillations of a DFIG and electromechanical oscillations are further examined, and alternative dampers are designed to suppress these oscillations [15]. The potential of imposing inter-area oscillation damping control with wind power plants is studied in [16]. The effect of spatial correlation between wind speed of geographically close wind farms on the damping of electromechanical oscillations is examined in [17]. With the aid of the wide area measurement system, a wide area damping controller is designed for DIFGs to alleviate electromechanical oscillations [18]. A second-order sliding-mode based damping controller is proposed in [19,20] as a resort for inter-area oscillation mitigation. A reduced-order model based optimal oscillation damping controller is also designed in [21]. A residue-based evaluation method is implemented to provide an additional control design for the power oscillations [22]. In addition, modulation and coordination resorts such as active power modulation and reactive power modulation [23] and DC-link control [24] are also proposed to damp inter-area oscillations with wind generation.

Apart from mitigating electromechanical oscillations with wind generation, the dynamic interaction between wind generation and the electromechanical dynamics has also drawn attention and is defined as a converter-driven stability problem [3]. Model validation and reduction techniques for different types of wind power induction generators (i.e., a fixed-speed induction generator (FSIG), DFIG) are discussed in terms of oscillatory stability issues [25–27]. The dynamic interaction between wind generation and the electromechanical modes of the nearby synchronous generators (SGs) poses threats to the small signal stability with high penetration levels of wind power, which is verified with modal analysis techniques [28]. An electric torque analysis method is proposed in [29] to quantify the impact of wind generation integration on electromechanical oscillations. A novel modal superposition theory is proposed in [30] to classify the interaction categories between wind generation and the external power system. The impact of power electronic integrated wind generation considering increasing wind penetration and load conditions on the inter-area oscillation is investigated in [31]. An adaptive coordination strategy is proposed in [32] to eliminate the modal resonance between FCWG dynamics and electromechanical dynamics.

Although the above works validated the impact of wind generation on electromechanical dynamics and provided satisfactory solutions to tackle the electromechanical oscillations with various control resorts, the systematic modeling to deepen the understanding of FCWG participation in electromechanical dynamics is still worth further exploring. Especially, an interesting phenomenon is discovered that, in some circumstances, the electromechanical oscillation mode (EOM) may be dominated by the FCWG dynamics and become a quasi-EOM, which has not been studied before. Therefore, the main contributions of this paper are summarized: (1) the linearized open-loop and closed-loop power system models tailored for FCWG dynamics impact investigation are established; (2) together with the electromechanical loop correlation ratio (ELCR), the FCWG dynamics correlation ratio (FDCR) and the quasi-ELCR (QELCR) are proposed to quantify the participation of FCWG in electromechanical dynamics; (3) extensive case studies considering comprehensive wind penetration levels are thoroughly examined to uncover the unusual transition in electromechanical dynamics; and (4) useful findings and suggestions on how FCWG dynamics transform both local and inter-area modes are provided based on modal analysis and time domain simulations.

The remainder of this paper is organized as follows. Section 2 presents a typical configuration of FCWG. Section 3 proposes a method to investigate the participation of FCWG by constructing the open-loop linearized power system model and the closed-loop linearized power system model. In Section 4, the participation of FCWG is meticulously examined in a two-area test system, and important findings on the impact of the electromechanical dynamics are concluded. The main findings are summarized in Section 5, while conclusions are emphasized in Section 6.

2. Configuration of FCWG

The typical topology of an FCWG (e.g., permanent magnet synchronous generator (PMSG)) connected to the multi-machine power system is demonstrated in Figure 1.

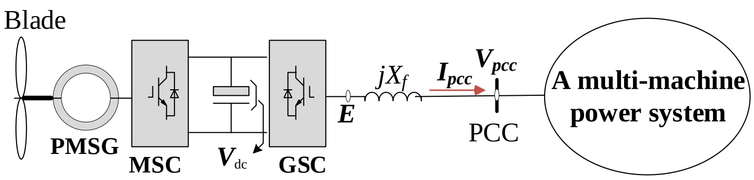

Figure 1. Physical configuration of a full converter-based wind power generation (FCWG) connected to a multi-machine power system.

The FCWG consists of three parts: (1) the PMSG, the machine side converter (MSC) and the associated control system (as demonstrated in Figure 2); (2) the DC-link, the grid side converter (GSC) and the associated control system (as shown in Figure 3); and (3) the synchronous reference frame phase-locked loop (SRF-PLL) (as presented in Figure 4), which is used to synchronize FCWG with the external power system.

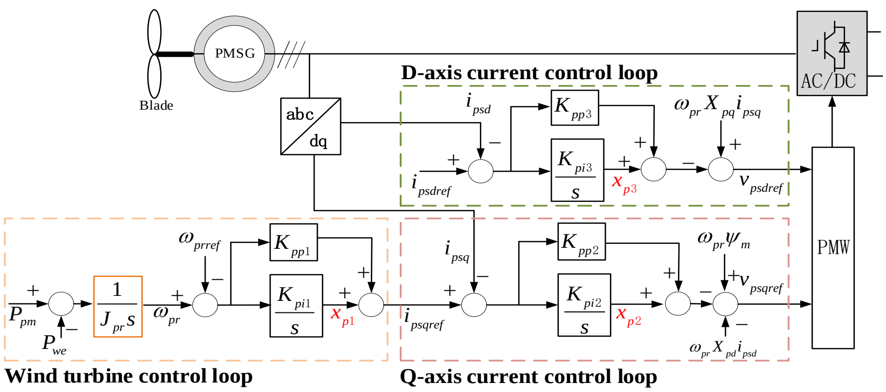

Figure 2. The control configuration of machine side converter (MSC).

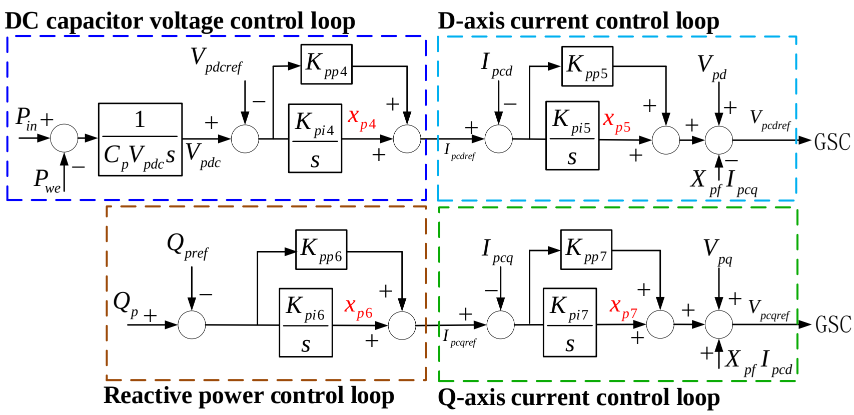

Figure 3. The control configuration of grid side converter (GSC).

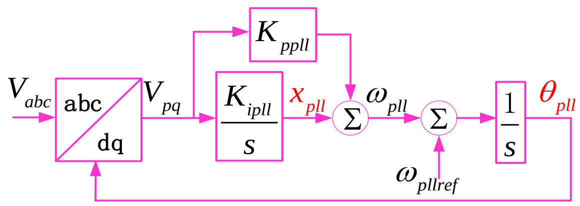

Figure 4. Block diagram of the synchronous reference frame phase-locked loop (SRF-PLL).

The electromechanical dynamics stem from the inertia sources of power systems. Regarding the large mass of physical rotors, SGs are the main inertia sources of conventional power systems, which actuate as a buffer under unintended disturbance contingencies and bolster the oscillatory stability. Owing to the AC-DC-AC configuration, the rotor inertia of wind turbine is decoupled from the multi-machine power system, and hence FCWG is normally regarded as a low-inertia source. Such low-inertia characteristic is significantly distinguished from conventional power sources. Therefore, the integration of FCWG is usually recognized to be inertia-less, which may not participate in electromechanical dynamics like SGs. Its impact on electromechanical dynamics is not taken into account meticulously.

3. Modal Analysis on Electromechanical Dynamics and FCWG Dynamics

Comprehensive modal analyses of the electromechanical oscillation modes (EOMs) are carried out to essentially reveal the participation mechanism of FCWG in electromechanical dynamics. To elaborate on the participation of FCWG, the power system that excludes the FCWG dynamics is denoted as the open-loop power system, while the entire system is the closed-loop power system. By comparing the EOMs of the open-loop and closed-loop power systems, the impact of FCWG is quantified.

3.1. State-Space Model of FCWG

The detailed modeling of FCWG can refer to [12,33]. The state-space model of FCWG is expressed as

$$\begin{cases} \frac{d}{dt}\Delta X_W = A_W \Delta X_W + B_W \Delta V_W \\ \Delta I_W = C_W \Delta X_W \end{cases} \tag{1}$$

where ΔX_W denotes all the state variables of FCWG (as illustrated in Figures 2–4); A_W, B_W, C_W are the state-space matrices after integrating all the linearized differential equations.

It is noteworthy that all the controller parameters of FCWG are included in Equation (1) and will be further integrated in the closed-loop power system in Section 3.3. Mathematically, this is how FCWG controller parameters affect the formation of the state matrix and thus influence the electromechanical dynamics of the external power system.

3.2. Open-Loop Power System

In the open-loop power system, FCWG is regarded as a constant power source, and thus its dynamics are excluded.

The state-space model of the i^{th} SG in the power system can be expressed as

$$\begin{cases} \frac{d}{dt}\Delta X_{gi} = A_{gi} \Delta X_{gi} + B_{gi} \Delta V_{gi} \\ \Delta I_{gi} = C_{gi} \Delta X_{gi} + D_{gi} \Delta V_{gi} \end{cases} \tag{2}$$

where ΔX_{gi} is the state variables of SG i; A_{gi}, B_{gi}, C_{gi}, D_{gi} are the state-space matrices; ΔV_{gi} and ΔI_{gi} are voltage variation and current variation at the connecting bus of SG i, respectively.

The equation of the transmission network is expressed as

$$\begin{bmatrix} \Delta I_g \\ 0 \end{bmatrix} = \begin{bmatrix} Y_{gg} & Y_{gN} \\ Y_{Ng} & Y_{NN} \end{bmatrix} \begin{bmatrix} \Delta V_g \\ \Delta V_N \end{bmatrix} = Y_{open} \begin{bmatrix} \Delta V_g \\ \Delta V_N \end{bmatrix} \tag{3}$$

where ΔI_g denotes the current variation at the generator buses; ΔV_g and ΔV_N are the voltage variations at the generator buses and other buses, respectively; Y_{open} is the open-loop admittance matrix of the transmission network in which the FCWG is considered as a constant power source and modeled as a constant impedance. Assume that the total number of SGs is M, then

$$\begin{aligned}
&\Delta I_g = \begin{bmatrix} \Delta I_{g1} & \Delta I_{g2} & \dots & \Delta I_{gM} \end{bmatrix}^T \\
&\Delta V_g = \begin{bmatrix} \Delta V_{g1} & \Delta V_{g2} & \dots & \Delta V_{gM} \end{bmatrix}^T \\
&\Delta X_g = \begin{bmatrix} \Delta X_{g1} & \Delta X_{g2} & \dots & \Delta X_{gM} \end{bmatrix}^T \\
&A_g = \mathrm{diag}\begin{bmatrix} \Delta A_{g1} & \Delta A_{g2} & \dots & \Delta A_{gM} \end{bmatrix}^T \\
&B_g = \mathrm{diag}\begin{bmatrix} \Delta B_{g1} & \Delta B_{g2} & \dots & \Delta B_{gM} \end{bmatrix}^T \\
&C_g = \mathrm{diag}\begin{bmatrix} \Delta C_{g1} & \Delta C_{g2} & \dots & \Delta C_{gM} \end{bmatrix}^T \\
&D_g = \mathrm{diag}\begin{bmatrix} \Delta D_{g1} & \Delta D_{g2} & \dots & \Delta D_{gM} \end{bmatrix}^T
\end{aligned} \tag{4}$$

where diag[] represents the diagonal matrix. By integrating all the SGs, the state-space model is expressed as

$$\begin{cases} \frac{d}{dt}\Delta X_g = A_g \Delta X_g + B_g \Delta V_g \\ \Delta I_g = C_g \Delta X_g + D_g \Delta V_g \end{cases} \tag{5}$$

From (3), the relationship between ΔI_g and ΔV_g can be expressed as

$$\Delta I_g = (Y_{gg} - \frac{Y_{gN} Y_{Ng}}{Y_{NN}}) \Delta V_g \tag{6}$$

Combine (5) and (6), and the state-space model of the open-loop power system is derived as

$$\frac{d}{dt}\Delta X_g = [A_g + \frac{B_g C_g}{Y_{gg} - \frac{Y_{gN} Y_{Ng}}{Y_{NN}} - D_g}] \Delta X_g = A_{open} \Delta X_g \tag{7}$$

where A_{open} is the state matrix of the open-loop power system.

3.3. Closed-Loop Power System

In the closed-loop power system, the dynamics of FCWG are included by injecting a current variation ΔI_W into the external power system. Accordingly, the network equation in Equation (3) should be modified as below

$$\begin{bmatrix} \Delta I_g \\ \Delta I_W \\ 0 \end{bmatrix} = \begin{bmatrix} Y_{gg} & Y_{gW} & Y_{gN} \\ Y_{Wg} & Y_{WW} & Y_{WN} \\ Y_{Ng} & Y_{NW} & Y_{NN} \end{bmatrix} \begin{bmatrix} \Delta V_g \\ \Delta V_W \\ \Delta V_N \end{bmatrix} = Y_{close} \begin{bmatrix} \Delta V_g \\ \Delta V_W \\ \Delta V_N \end{bmatrix} \tag{8}$$

where ΔI_g and ΔI_W are the current variations at generator buses and the FCWG bus, respectively; ΔV_g, ΔV_W and ΔV_N are the voltage variations at generator buses, FCWG bus, and other buses; and Y_{close} is the admittance matrix of the transmission network.

Eliminating the non-source buses, the network equation can be simplified as

$$\begin{bmatrix} \Delta I_g \\ \Delta I_W \end{bmatrix} = \begin{bmatrix} Y_{gg} - \frac{Y_{gN}Y_{Ng}}{Y_{NN}} & Y_{gW} - \frac{Y_{gN}Y_{NW}}{Y_{NN}} \\ Y_{Wg} - \frac{Y_{WN}Y_{Ng}}{Y_{NN}} & Y_{WW} - \frac{Y_{WN}Y_{NW}}{Y_{NN}} \end{bmatrix} \begin{bmatrix} \Delta V_g \\ \Delta V_W \end{bmatrix} = \begin{bmatrix} Y_{11} & Y_{12} \\ Y_{21} & Y_{22} \end{bmatrix} \begin{bmatrix} \Delta V_g \\ \Delta V_W \end{bmatrix} \tag{9}$$

From the second equation of (1), the second equation of (5), and (9), the relation between voltage variation and the state variables is expressed as

$$\begin{bmatrix} \Delta V_g \\ \Delta V_W \end{bmatrix} = \begin{bmatrix} Y_{11} - D_g & Y_{12} \\ Y_{21} & Y_{22} \end{bmatrix}^{-1} \begin{bmatrix} C_g & C_W \end{bmatrix} \begin{bmatrix} \Delta X_g \\ \Delta X_W \end{bmatrix} \tag{10}$$

From the first equations of (1) and (5),

$$\frac{d}{dt}\begin{bmatrix} \Delta X_g \\ \Delta X_W \end{bmatrix} = \begin{bmatrix} A_g & 0 \\ 0 & A_W \end{bmatrix} \begin{bmatrix} \Delta X_g \\ \Delta X_W \end{bmatrix} + \begin{bmatrix} B_g & 0 \\ 0 & B_W \end{bmatrix} \begin{bmatrix} \Delta V_g \\ \Delta V_W \end{bmatrix} \tag{11}$$

From (10) and (11), the closed-loop state-space model of the entire power system is derived as

$$\frac{d}{dt}\begin{bmatrix} \Delta X_g \\ \Delta X_W \end{bmatrix} = A_{closed} \begin{bmatrix} \Delta X_g \\ \Delta X_W \end{bmatrix} \tag{12}$$

where A_{closed} is state matrix of the closed-loop power system considering the dynamics of FCWG and is defined as

$$A_{closed} = \begin{bmatrix} A_g & 0 \\ 0 & A_W \end{bmatrix} + \begin{bmatrix} B_g & 0 \\ 0 & B_W \end{bmatrix} \begin{bmatrix} Y_{11} - D_g & Y_{12} \\ Y_{21} & Y_{22} \end{bmatrix}^{-1} \begin{bmatrix} C_g & C_W \end{bmatrix} \tag{13}$$

By performing modal analysis on the state matrices of the open-loop and closed-loop power systems and comparing all the essential information of the oscillation modes, the impact of FCWG dynamics can be revealed. One advantageous aspect of modal analysis is that it can give insight into the relationship between oscillation modes and physical components and reveal the interaction between FCWG dynamics and electromechanical dynamics. For example, by analyzing the participation factors of SGs, the local EOMs and the inter-area EOM can be identified [34,35]. Moreover, it is also easy to uncover those state variables and the corresponding controllers that are the most active in the interaction between electromechanical dynamics and FCWG dynamics via the same technique.

3.4. Impact of FCWG on Electromechanical Dynamics

The EOMs are identified with the electromechanical loop correlation ratio (ELCR), which is defined as

$$ELCR = \frac{PF_{rotor}}{PF_{total} - PF_{rotor}} \tag{14}$$

where PF_{rotor} is the sum of participation factors (PFs) related to electromechanical oscillatory loop associated with state variables (i.e., the rotor speed ω and rotor angle δ) for all M SGs, and PF_{total} is the sum of PFs of all state variables.

For any oscillation mode, if its ELCR is larger than 1, the oscillation mode is identified to be an EOM. Similarly, the FCWG dynamic correlation ratio (FDCR) can also be proposed to distinguish FCWG oscillation modes, which is defined as

$$FDCR = \frac{PF_{FCWG}}{PF_{total} - PF_{FCWG}} \tag{15}$$

where PF_{FCWG} is the sum of participation factors (PFs) related to all state variables of FCWG.

Since the MSC of FCWG is decoupled from the external power system, the most interactive part is the grid side converter (GSC) of FCWG, and it should be highlighted that the concept of FDCR can be extended to any other power source (e.g., voltage source converter (VSC)). Likewise, the methodology proposed in this paper can be applied to study the impact on electromechanical dynamics from any kind of converter-based power sources (such as PV, energy storage system (ESS)).

In an EOM, two state variables (i.e., the rotor speed ω and rotor angle δ) related to the SG rotor are recognized as the main contributors to electromechanical oscillatory dynamics. For FCWG, there are usually two state variables taking part in the EOM most actively when strong interaction happens. Normally, a pair of state variables, which is closely related to a controller of FCWG (e.g., PLL controller, or DC voltage controller), might participate actively in electromechanical dynamics, and thus can be regarded as quasi-electromechanical state variables. Though these state variables are not from any physical rotational storage, their participation in an EOM will inevitably affect the electromechanical dynamic responses and might incur unintended consequences if not properly tackled.

If strong interaction between FCWG and the external power system occurs, the quasi-electromechanical state variables may hold a considerable PF in an EOM, and thus ELCR in Equation (14) may fall below 1. As a result, ELCR is not suitable for identifying EOMs in such cases. To fill in this gap, a quasi-ELCR (QELCR) is proposed to account for the two quasi-electromechanical state variables and is defined as

$$QELCR = \frac{PF_{rotor} + PF_{QEWG}}{PF_{total} - PF_{rotor} - PF_{QEWG}} \tag{16}$$

where PF_{QEWG} is the sum of PFs of the two quasi-electromechanical state variables from FCWG.

For any oscillation mode with an FDCR larger than 1, it can be recognized as an FOM. By analyzing the ELCR and FDCR of the same EOM, it is possible to quantify the participation of FCWG. Normally, the dynamics of FCWG are not involved in the EOM, and thus it is straightforward to identify an EOM via ELCR. However, if FCWG dynamics are strongly coupled with the electromechanical dynamics, ELCR may be lower than 1. Hence, ELCR is no longer suitable for EOM identification. In such a situation, two possible results may emerge: 1) the electromechanical dynamics may mingle with the FCWG dynamics; an EOM may be dominated by FCWG dynamics instead of the rotors of SGs, and is no longer a typical EOM, and thus can be identified as a quasi-EOM; and 2) a new quasi-EOM may be introduced (which may also be dominated by FCWG) and imposed on the rotor swing movements of SGs. To be more specific, a very interesting phenomenon may appear, in which, with the increase of the FDCR and the decrease of the ELCR, a typical EOM will gradually turn into a quasi-EOM, and at the same time, the most interactive FOM may have an ELCR larger than 1, and can be considered as a new quasi-EOM. Such a transition from the electromechanical dynamics to the quasi electromechanical dynamics is rare but may occur if FCWG strongly interacts.

With the criteria of ELCR and FDCR, it is capable of distinguishing all the EOMs and FOMs, as presented in Figure 5. This mode identification criteria can be implemented to observe the unusual transition in electromechanical dynamics.

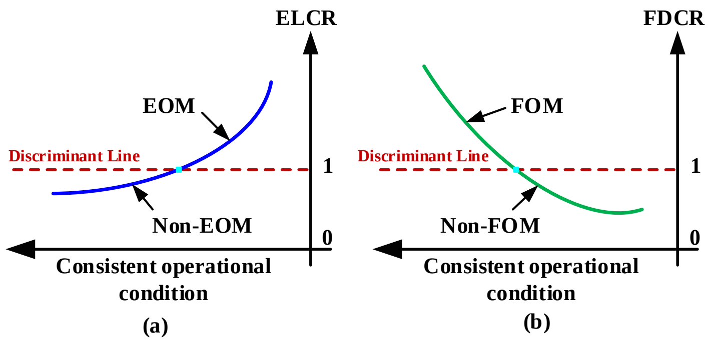

Figure 5. Criteria for electromechanical oscillation mode (EOM) and FCWG oscillation mode (FOM) identification: (**a**) EOM identification; (**b**) FOM identification.

4. Case Study

4.1. Introduction of Test System

An FCWG-integrated modified two-area power system is set up as a test system for investigation, as illustrated in Figure 6, in which the FCWG-based wind farm is connected at bus 12. Busbar 3 is the swing bus of the test system. To emulate the electromechanical dynamics, the simplified third-order model with a first order of the automatic voltage regulator (AVR) is adopted for each SG. No power system stabilizer (PSS) is equipped. All the parameters of SGs in [34] and the parameters of FCWG in [12] are used, and a detailed mathematical model can be found in [12,34].

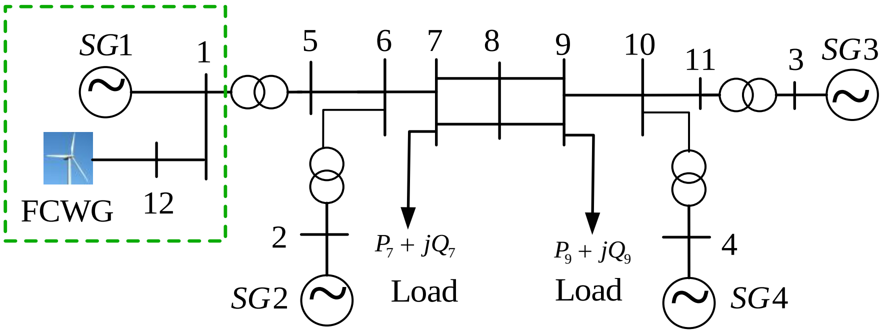

Figure 6. Configuration of two-area power system integrated with an FCWG wind farm.

To cover the participation level, the FCWG is used to replace the active power of SG1 step by step. The total active power output of FCWG and SG1 is 600 MW and kept constant. Other SGs and network and load parameters are the same throughout the following study.

The proportion of FCWG active power output increases from 0% to 100% with a change step of 2% (i.e., 12 MW). Meanwhile, the active power of SG1 decreases from 100% to 0% with the same amount of change step. To simplify the expression, "FCWG proportion" is used to represent the active power share of FCWG in the total active power of FCWG and SG1 (i.e., 600 MW). A higher FCWG proportion also indicates a higher wind power penetration level.

The impact of FCWG on all the EOMs are analyzed through modal analysis. Mathematically, the dynamic interaction between FCWG and the external power system can be seen as a modal coupling in which a major FOM interacts with the EOMs of the external power system. In other words, some state variables (usually two) of FCWG may participate in the EOMs, and state variables of rotor dynamics of SGs may also take part in the FOM that is determined by these FCWG state variables.

The original EOMs of the two-area power system (i.e., the output of FCWG is Pew = 0%) are identified and presented in Table 1.

Table 1. Electromechanical oscillation modes (EOMs) of two-area power system (Pew = 0.0%).

EOM No.	EOM1	EOM2	EOM3
Eigenvalue λ	−0.0660 ± 3.3891i	−0.3201 ± 5.7346i	−0.2824 ± 5.9767i
Freq. (Hz)	0.5394	0.9127	0.9512
Damping Ratio	1.95%	5.57%	4.72%
Electromechanical loop correlation ratio (ELCR)	9.3952	23.7402	17.4803
FCWG dynamic correlation ratio (FDCR)	0	0	0
Major sources	SG3, SG4, SG1, SG2	SG2, SG1	SG4, SG3

The participation of power sources is also compared and demonstrated to clarify the relationship between the EOM and power sources, as shown in Figure 7. EOM1 is an inter-area oscillation mode that all SGs take part in, while EOM2 and EOM3 are two local oscillation modes that are dominated by

SG1, SG2, and SG3, SG4, respectively. Since FCWG is integrated into the left area, it is much more likely that FCWG will participate in two EOMs (i.e., EOM1 and EOM2) and will not affect EOM3.

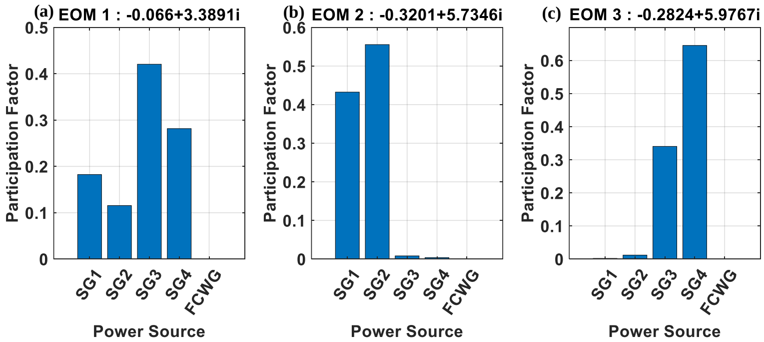

Figure 7. The participation of power sources in EOMs: (**a**) EOM1; (**b**) EOM2; (**c**) EOM3.

The participation of FCWG in the EOM is not only affected by the power injection level, but is also impacted by the parameters of the FCWG controllers. The interaction between FCWG and the external power system is strongly related to the relative locations of the FOM and the EOM. For a specific power system, EOMs normally do not vary too much and will stay at relatively stable frequencies. Meanwhile, the location of FOM is mainly determined by the controller parameters and operating conditions. The former is decisive as controller parameters can be designed with bandwidth to accommodate signals of various oscillation frequencies. While the latter also affects the FOM location with different power flows, such relation may not be decisive since it is mainly attributed to the variation of voltage and current, which are not strongly coupled in controller oscillation modes.

To give a thorough demonstration, two FOMs are selected to interact with the EOMs, i.e., the PLL-FOM which denotes the dynamics of the PLL controller, and the DC-FOM which represents the dynamics of the DC voltage controller. Different PI parameters are selected and denoted as different scenarios (under a 50% FCWG penetration level), as presented in Tables 2 and 3.

Table 2. Different scenarios with respect to PLL-FOM under 50% FCWG penetration level.

Scenario No.	Parameters of PLL Controller	PLL-FOM	EOM1	ELCR	FDCR
Scen. 1	Kipll = 6, Kppll = 1	−0.5243 ± 2.4481i	−0.1712 ± 3.4044i	9.8518	0.0260
Scen. 2	Kipll = 8, Kppll = 1	−0.5057 ± 2.8071i	−0.1851 ± 3.4137i	7.2631	0.0601
Scen. 3	Kipll = 10, Kppll = 1	−0.4627 ± 3.1275i	−0.2233 ± 3.4200i	3.6326	0.1793
Scen. 4	Kipll = 12, Kppll = 1	**−0.4412 ± 3.5208i**	**−0.2397 ± 3.3226i**	**2.3364**	**0.2905**
Scen. 5	Kipll = 14, Kppll = 1	−0.4870 ± 3.7901i	−0.1889 ± 3.3257i	4.4731	0.1148
Scen. 6	Kipll = 16, Kppll = 1	−0.4986 ± 4.0331i	−0.1724 ± 3.3359i	6.1709	0.0632
Scen. 7	Kipll = 100, Kppll = 1	−0.4364 ± 9.8689i	−0.1559 ± 3.3686i	11.7832	0.0023

Table 3. Different scenarios with respect to DC-FOM under the 50% FCWG penetration level.

Scenario No.	Parameters of DC Voltage Controller	DC-FOM	EOM1	ELCR	FDCR
Scen. 8	Kpi4 = 100, Kpp4 = 2	−0.0955 ± 1.8304i	−0.1614 ± 3.3743i	11.5318	0.0061
Scen. 9	Kpi4 = 200, Kpp4 = 2	−0.1558 ± 2.5672i	−0.1777 ± 3.3826i	8.8525	0.0340
Scen. 10	Kpi4 = 300, Kpp4 = 2	**−0.1651 ± 3.0997i**	**−0.2500 ± 3.4155i**	**2.1014**	**0.3827**
Scen. 11	Kpi4 = 400, Kpp4 = 2	−0.3863 ± 3.6959i	−0.1136 ± 3.2919i	3.0269	0.1943
Scen. 12	Kpi4 = 500, Kpp4 = 2	−0.4665 ± 4.0728i	−0.1201 ± 3.3287i	5.9994	0.0612
Scen. 13	Kpi4 = 600, Kpp4 = 2	−0.5485 ± 4.4338i	−0.1257 ± 3.3402i	7.7275	0.0316
Scen. 14	Kpi4 = 2000, Kpp4 = 2	−1.8423 ± 7.9388i	−0.1359 ± 3.3565i	10.5869	0.0053

For Scenarios 1–7, only the parameters of the PLL controller change, and all other parameters of FCWG stay at their original values. For Scenarios 8–14, only the parameters of the DC voltage controller vary, and all other parameters remain unchanged. It should be noted that the controller parameters are included in Equation (13), and the variation of these parameters will affect the state matrix A_{closed} and thus influence the eigenvalue of the EOMs. When controller parameters change, ELCR and FDCR also vary. Among all the scenarios, it is interesting that Scenario 4 and Scenario 10 have the lowest ELCR and the highest FDCR in the corresponding tables. This implies that in Scenario 4 and Scenario 10, FCWG dynamics are more active in interacting with the electromechanical dynamics. The decrease of ELCR and the increase of FDCR may lead to the transition in electromechanical dynamics. If the ELCR falls below 1, the unusual transition occurs, and thus an EOM will turn into a quasi-EOM, which will be demonstrated in Sections 4.2 and 4.3.

Comparing the FOMs in Tables 2 and 3, the oscillation frequencies of FOMs increase with the integral parameter of the controllers. When the oscillation frequencies of FOMs are close to the frequency of EOM1 (about 0.5 Hz), the participation of FCWG becomes very active. When the FOMs move away, the participation of FCWG becomes less active.

4.2. Interaction Between PLL-FOM and EOMs

Modal analyses are extensively implemented for every scenario, considering 50 operating conditions (0–100% penetration level of FCWG). For each group of controller parameters, eigenvalue analyses are implemented based on varying operating conditions and thus the eigenvalue loci of critical modes are drawn, which are significantly different from the parameter-based root locus. Therefore, the term "eigenvalue loci" is used in this paper to distinguish from "root locus".

The interactions between PLL-FOM and EOM1, EOM2 are demonstrated in Figures 8 and 9, respectively. It is worth mentioning that EOM3 is hardly influenced by the integration of FCWG since it is another local EOM which is closely related to SG3 and SG4, and thus is not presented due to space limit.

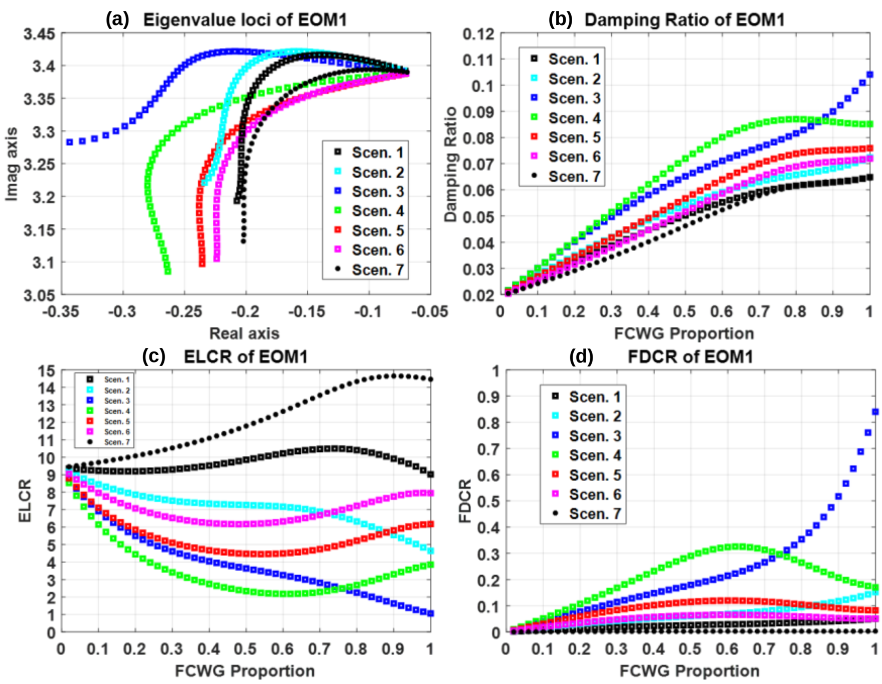

Figure 8. The interaction between PLL-FOM and EOM1 considering increasing FCWG proportion: (**a**) eigenvalue loci; (**b**) variation trend of damping ratio; (**c**) variation trend of ELCR; (**d**) variation trend of FDCR.

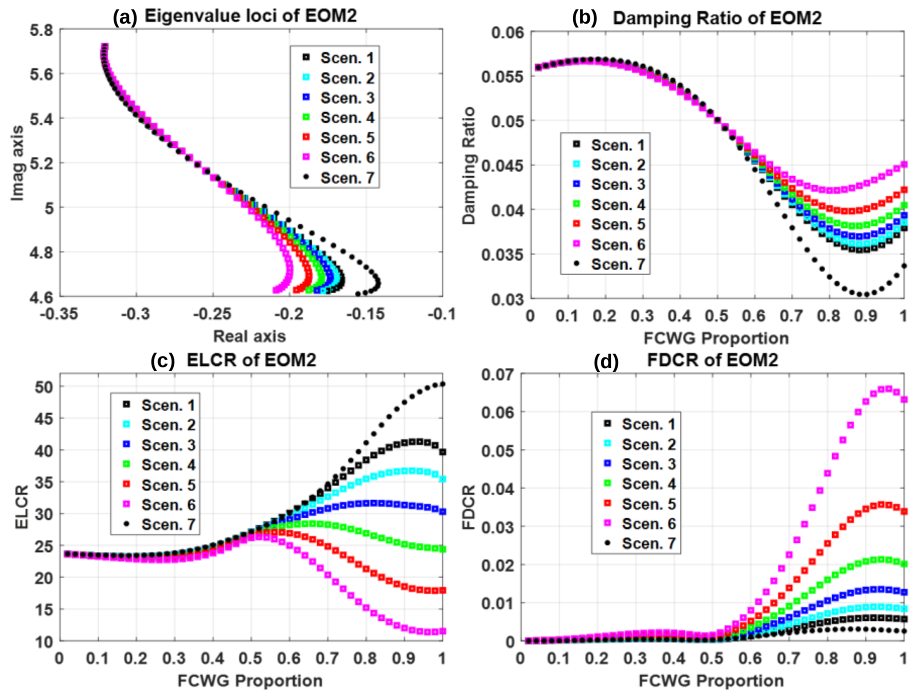

Figure 9. The interaction between PLL-FOM and EOM2 considering increasing FCWG proportion: (**a**) eigenvalue loci; (**b**) variation trend of damping ratio; (**c**) variation trend of ELCR; (**d**) variation trend of FDCR.

In Scenarios 1–7, the integration of FCWG is beneficial for EOM1, as it is shown that in Figure 8a, the eigenvalue of EOM1 turns to move towards the left in the complex plane, and Figure 8b further confirms that the damping ratio of EOM1 is enhanced. It is very interesting that, in Figure 8c, the ELCR may increase or decrease under different scenarios. Particularly, for Scenario 3, the ELCR continuously decreases to almost 1 when the FCWG proportion is near 100%, which indicates that EOM1 gradually interacts with FCWG dynamics while the electromechanical dynamics become less and less active. At the same time, the FDCR increases from 0 to almost 1. If ELCR falls below 1 and FDCR is above 1, the corresponding EOM will transform into a quasi-EOM.

Moreover, the FDCR in Figure 8d demonstrates that in most scenarios, the participation of FCWG in EOM1 stays at a low level (e.g., for Scenarios 1, 2, 5, 6, and 7, FDCR is less than 0.1), which suggests that the dynamic interaction is weak, and the damping enhancement is largely due to the power injection of FCWG. However, the FDCRs can increase drastically in Scenarios 3 and 4, and the damping ratio can also be raised a lot when FCWG participates actively. This indicates that dynamic interaction could be too strong to be ignored. It is surprising that such dynamic interaction is positive and may be utilized as a resort to enhance oscillatory stability.

From Figure 8, it is concluded that strong interaction between FCWG and the external power system is possible. In this case, the integration of FCWG is conducive for EOM1, and the damping ratio of the EOM is raised from 1.95% to over 10%, which is prominent from the perspective of low frequency oscillation suppression.

In Scenarios 1–7, the overall impact of FCWG integration is negative for EOM2, as it is shown that in Figure 9a, the eigenvalue of EOM1 tends to move towards the right in the complex plane, and Figure 9b further confirms that the damping ratio of EOM1 decreases.

The ELCRs in Figure 9c encounter some fluctuations under different scenarios, but stay above 10 all the time, which means EOM2 is always dominated by electromechanical dynamics, whereas the FDCRs in Figure 9d are always less than 0.1, which indicates the participation of FCWG dynamics is very limited or even can be ignored. This finding elucidates that the damping deterioration of EOM2 is mainly attributed to the power injection of FCWG and the power reduction of SG1.

From Figure 9, it is concluded that the FCWG dynamics may not always hold considerable participation in the EOMs, and the power injection may become the main influence. The damping ratio of EOM2 decreases from 5.57% to about 3%, which is a potential threat for this local EOM. Careful coordination for FCWG integration should be considered.

4.3. Interaction Between DC-FOM and EOMs

From the analyses in Section 4.2, the parameters of the PLL controller play an important role in the interaction between FCWG dynamics and electromechanical dynamics. With certain parameters in the PLL controller, FCWG can have very active participation in electromechanical dynamics (e.g., Scenarios 3 and 4).

To further validate the participation of FCWG, the parameters in the DC voltage controller are also examined to investigate the interaction of DC-FOM and the EOMs. Accordingly, Scenarios 8–14 are studied via modal analysis, considering 50 operating conditions (which covers from 0% to 100% penetration level of FCWG with a 2% step). The results of the interaction between DC-FOM and EOM1, EOM2 are depicted in Figure 10 and Figure 11, respectively.

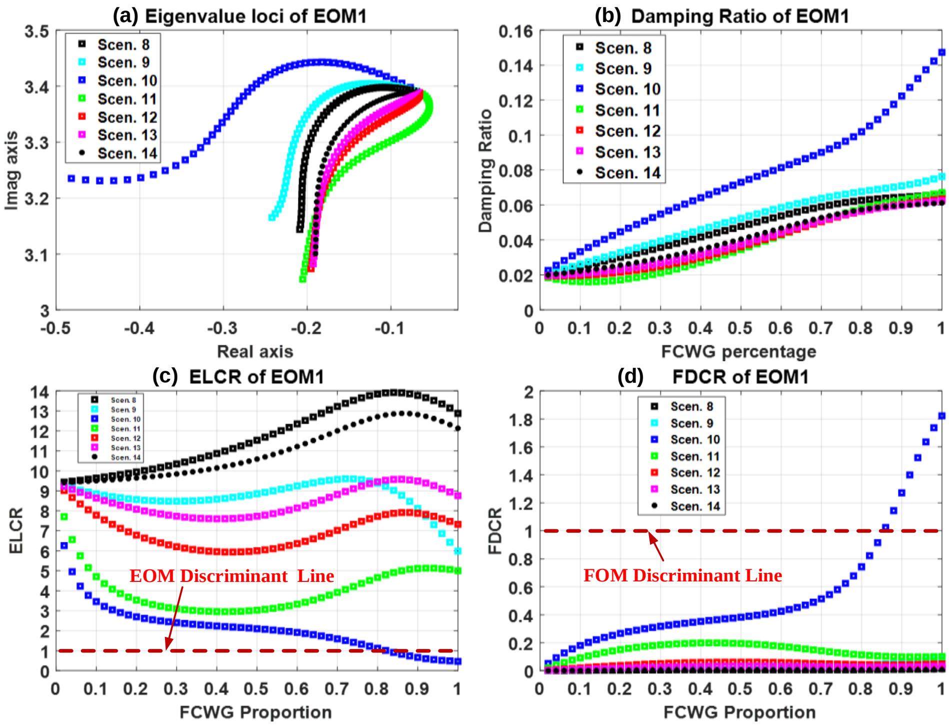

Figure 10. The interaction between DC-FOM and EOM1, considering increasing FCWG proportion: (**a**) eigenvalue loci; (**b**) variation trend of damping ratio; (**c**) variation trend of ELCR; (**d**) variation trend of FDCR.

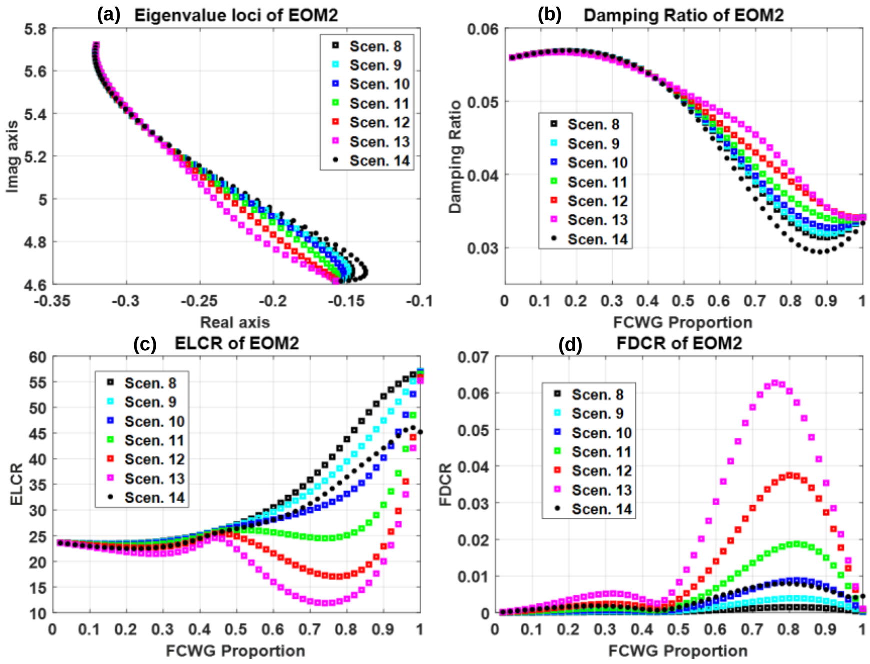

Figure 11. The interaction between DC-FOM and EOM2, considering increasing FCWG proportion: (**a**) eigenvalue loci; (**b**) variation trend of damping ratio; (**c**) variation trend of ELCR; (**d**) variation trend of FDCR.

In Scenarios 8–14, the overall impact of FCWG integration is also beneficial for EOM1, as it is shown that in Figure 10a, the eigenvalue of EOM1 tends to move towards the left in the complex plane. Figure 10b further ascertains that the damping ratio of EOM1 is enhanced.

In Figure 10c, the ELCR may also increase or decrease under different scenarios, which is similar to that of Figure 8c. However, when it comes to ELCRs and FDCRs, it should be highlighted that, for Scenario 10, the ELCR consistently decreases to below 1, which implies that EOM1 is no longer a typical EOM that is determined by the electromechanical dynamics, and the participation of FCWG becomes the primary domination. As also verified in Figure 10d, the FDCR in Scenario 10 can increase to above 1 at the 86% penetration level, which also indicates this oscillation mode (i.e., previously identified to be EOM1) now becomes a quasi-EOM.

It is worth pointing out that, although all scenarios can improve the damping ratio of EOM1, the contribution of damping enhancement due to FCWG integration are from two aspects: (1) the power flow impact (which refers to the low participation of FCWG, such as in Scenarios 8–9, 12–14); and (2) dynamic interaction impact (which could superpose dynamic impact on the electromechanical dynamics and even dominate the electromechanical oscillatory stability, such as in Scenario 10).

In Scenario 10, the integration of FCWG is conducive for EOM1, and the damping ratio of EOM1 can be raised from 1.95% to about 15%, which is quite impressive comparing with other scenarios (which can only reach about 8% damping ratio). This proves that dynamic interaction can be pronounced and should not be ignored, and the participation of FCWG is significant.

The interaction between DC-FOM and EOM2 is shown in Figure 11. The damping ratio of EOM2 decreases in all scenarios, which indicates that the integration of FCWG is negative for EOM2. Such influence is mainly attributed to the power flow impact of FCWG, since the FDCRs are at a very low level (less than 0.1 as illustrated in Figure 11d). Though the ELCRs in Figure 11c have encountered fluctuations, they stay at a very high level (over 10), and thus the electromechanical dynamics of EOM2 are hardly affected by FCWG dynamics.

Peculiarly, take Scenario 10 as an example, major modes related to electromechanical dynamics in both an open-loop power system and a closed-loop power system model are demonstrated in Table 4 (the FCWG proportion is 86%). Due to the strong interactions between FCWG dynamics and electromechanical dynamics, there are only two typical EOMs (i.e., EOM2 and EOM3) left in the closed-loop power system. The inter-area EOM 1 (i.e., 0.51 Hz) is now dominated by FCWG with an ELCR less than 1 and an FDCR larger than 1, and thus is a quasi-EOM. Local EOM2 is slightly affected while local EOM3 is hardly moved by comparing them with the closed-loop modes 3 and 4. The participation of power sources in four major oscillation modes is depicted in Figure 12. It is worthwhile mentioning that the active participation of FCWG not only dominates the inter-area mode (viz. Closed Mode 2) but also introduces a new quasi-EOM (i.e., Closed Mode 1), in which the electromechanical dynamics are involved.

Table 4. EOMs of two-area power system in Scenario 10 (Pew = 86%).

Mode No.	Eigenvalue λ	Freq. (Hz)	Damping Ratio	ELCR	FDCR
Open-Loop Power System					
Open EOM1	−0.1994 ± 3.2280i	0.5138	6.17%	17.4809	0
Open EOM2	−0.1677 ± 4.7219i	0.7515	3.55%	47.7340	0
Open EOM3	−0.2839 ± 5.9764i	0.9512	4.75%	17.9009	0
DC-FOM	−0.5333 ± 3.1585i	0.5027	16.65%	0	6.3587
Closed-Loop Power System					
Closed Mode 1	−0.2777 ± 3.0665i	0.4880	9.02%	**0.8911**	**0.8601**
Closed Mode 2	−0.3697 ± 3.2492i	0.5171	11.31%	**0.8194**	**1.0237**
Closed Mode 3	−0.1563 ± 4.6983i	0.7478	3.33%	36.6454	0.0084
Closed Mode 4	−0.2840 ± 5.9762i	0.9511	4.75%	17.8584	0

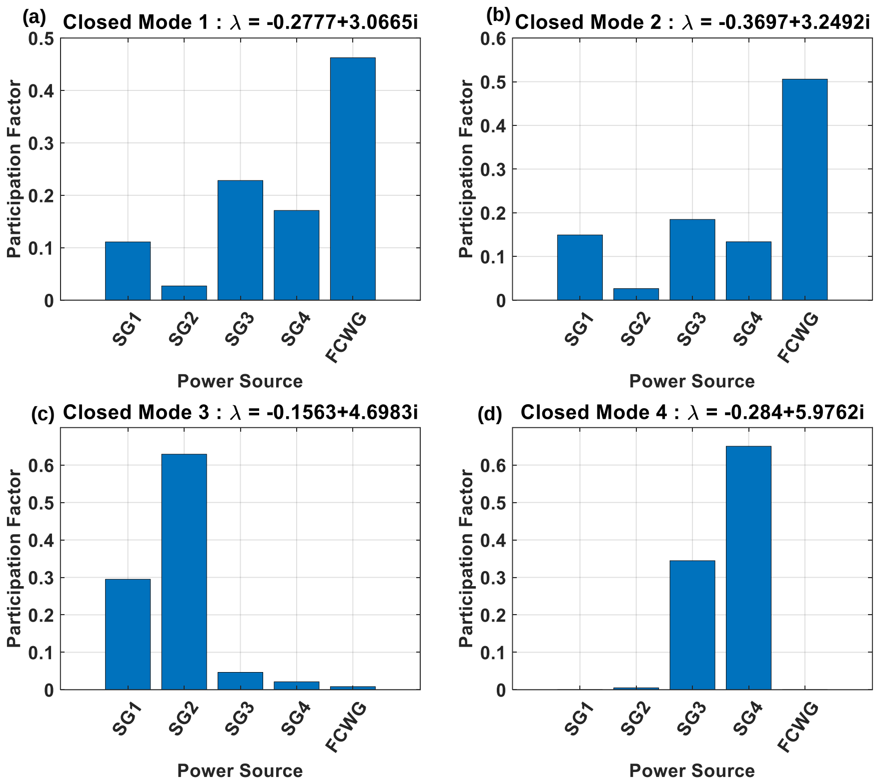

Figure 12. The participation of power sources in major oscillation modes of the closed-loop power system: (**a**) closed-loop Mode 1; (**b**) closed-loop Mode 2; (**c**) closed-loop Mode 3; (**d**) closed-loop Mode 4.

4.4. Time Domain Simulations for Verification of Frequency Domain Analysis

From the analysis above, in Scenario 4 and Scenario 10, FCWG has the most active participation. To verify the above analyses, time domain simulations are also performed. The simulation condition is set: a 5% increase of mechanical output occurs at SG2 at 0.2 s and then drops to the original value after 100 ms. The FCWG penetration level is set to be 50% (i.e., 300 MW), and all the parameters of the transmission network and generators are the same. To save space and maintain clarity, only Scenarios 4, 7, and 10 are selected to implement the small disturbance simulations.

The angular speed, bus voltage, and active power of SG3 are compared in Figure 13a–c. The reason why variables of SG3 are chosen for comparison is that, in time domain simulations, the variation of SG3 variables are formulated with the superposition of both local mode (EOM3) and inter-area mode (EOM1). The participation of FCWG affects both EOM1 and EOM2, whereas FCWG integration benefits EOM1 and deteriorates EOM2 at the same time, and these two EOMs will impose on the dynamic performances of SG1 and SG2 and may lead to misunderstanding. Therefore, by comparing variables of SG3 under different scenarios, the impact on EOM1 from the participation of FCWG can be clearly demonstrated.

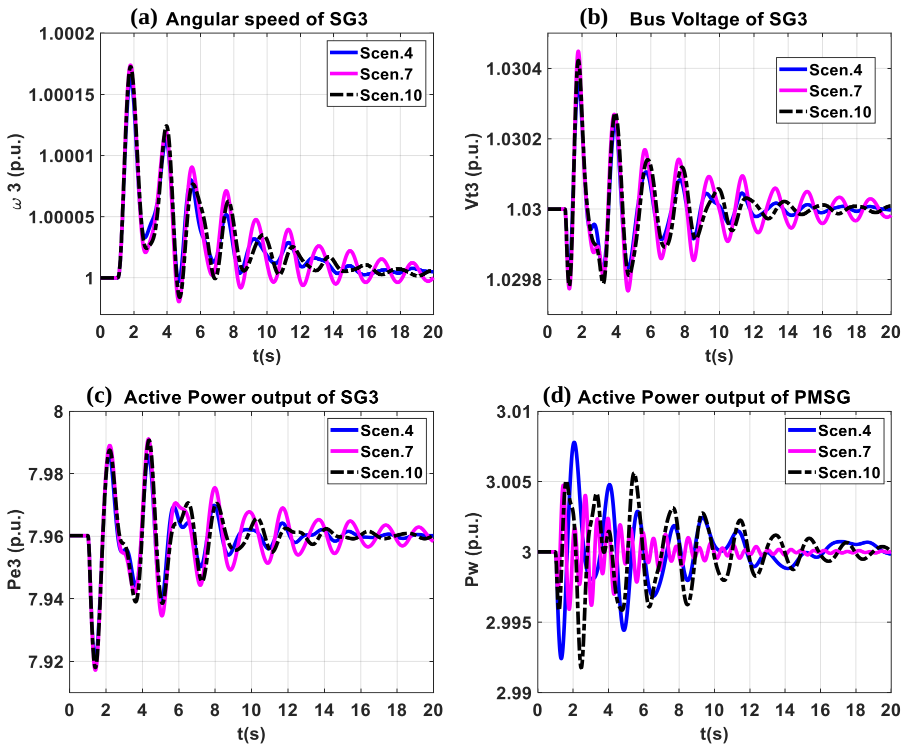

Figure 13. The dynamic responses of interaction between FCWG dynamics and electromechanical dynamics: (**a**) angular speed of SG3; (**b**) bus voltage of SG3; (**c**) active power of SG3; (**d**) active power of FCWG.

Scenarios 4 and 10 have better dynamic performances than that of Scenario 7 in terms of electromechanical dynamics. The only difference is whether FCWG actively participates or not. It is important to also mention that the participation of FCWG in electromechanical dynamics may introduce negative effects on its own dynamics. For example, the active powers of FCWG in Scenarios 4 and 10 have worse dynamic performances than that of Scenario 7, as demonstrated in Figure 13d. Therefore, the integration of FCWG may not only participate in the electromechanical dynamics and influence the oscillatory stability of the power system; additionally the side effects of its own dynamic performances should also be carefully considered. Appropriate coordination between FCWG dynamics and electromechanical dynamics is suggested when integrating FCWG into the power system.

4.5. Discussion on a Special Case: Replacement of SG with FCWG

The replacement of an SG with FCWG significantly affects the electromechanical dynamics. On one hand, with the removal of an SG from the grid, the rotor swing dynamics of this SG are now excluded from the inter-area EOM. On the other hand, a local EOM closely related to this SG may also disappear (e.g., EOM 2 of the two-area benchmark system in this paper). In a weak interaction case, FCWG hardly interacts with electromechanical dynamics, and hence the replacement of SG1 with FCWG will lead to the disappearance of the local EOM between SG1 and SG2, as confirmed in Figure 14. There are only two EOMs left in the power system, i.e., a local EOM associated with SG3 and SG4, and the inter-area EOM in which the remaining three SGs participate.

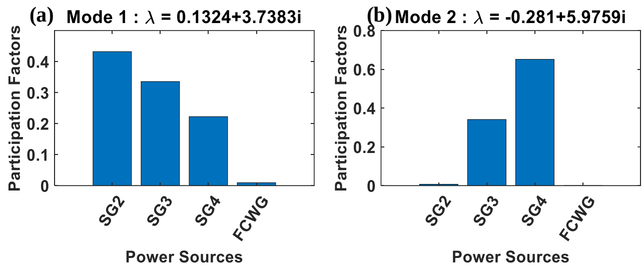

Figure 14. Weak interaction case: participation of power sources in EOMs when SG1 is replaced with FCWG: (**a**) closed-loop Mode 1; (**b**) closed-loop Mode 2.

However, if strong interaction between FCWG and the external power system occurs, two quasi-electromechanical state variables of FCWG may act as the electromechanical oscillatory loop associated state variables of the replaced SG, and hence introduce a new local quasi-EOM. In such circumstances, the integration of FCWG becomes vital in determining power system oscillatory stability. As demonstrated in Figure 15, the local EOM (Mode 4) and the inter-area EOM (Mode 3) still exist. FCWG could have a significant participation in the inter-area EOM (Mode 3) due to the active interaction between FCWG and electromechanical dynamics, which may pose threats to the power system oscillatory stability if not properly tackled. Moreover, two quasi-EOM are introduced (Mode 1 and Mode 2). Mode 1 can be regarded as a local quasi-EOM, since it is mainly dominated by SG2 and FCWG. Meanwhile, Mode 2 is largely a FOM, whereas all 3 SGs participate actively, and hence can also be recognized as an inter-area quasi-EOM.

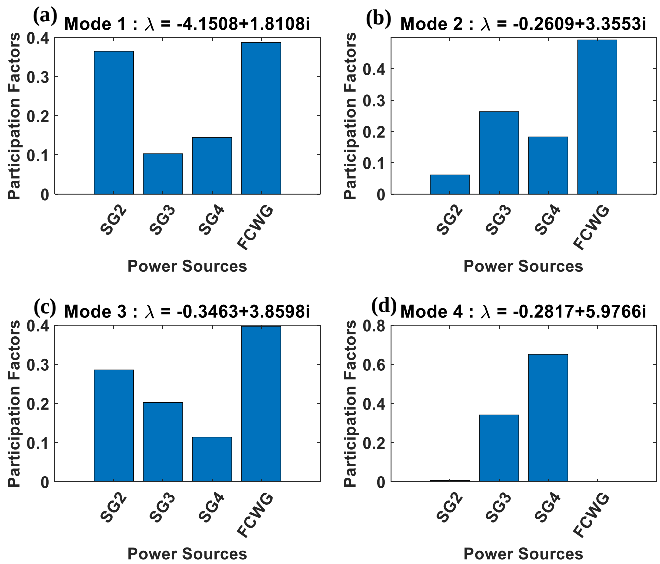

Figure 15. Strong interaction case: participation of power sources in EOMs when SG1 is replaced with FCWG: (**a**) closed-loop Mode 1; (**b**) closed-loop Mode 2; (**c**) closed-loop Mode 3; (**d**) closed-loop Mode 4.

Above all, the replacement of SG with FCWG should be carefully investigated. In the weak interaction case, it normally leads to the missing of a local EOM, while in the strong interaction case, new quasi-EOMs may be introduced. Such impact on the electromechanical dynamics may be critical for oscillatory stability and hence should be carefully tackled.

5. Discussion

Based on all the analyses above, some key findings with respect to the FCWG participation in electromechanical dynamics are summarized as below:

(1) FCWG dynamics might interact with both inter-area EOMs and local EOMs;
(2) The interaction can be either positive or negative, and may improve one EOM while deteriorate the other;
(3) Different FOMs with respect to different FCWG controllers may interact with the EOMs;
(4) For the same FCWG controller, the integral parameter plays a key role in determining the oscillation frequency of the relevant FOM and thus affects the participation of FCWG in the electromechanical dynamics;
(5) The degree of interaction is normally influenced by the penetration level of FCWG and the distance between the two affected modes. A strong interaction is more likely to occur at a high penetration level of FCWG, with the frequency of the FOM within the oscillation frequency range of the EOM (i.e., 0.2Hz–2.5Hz), especially when an FOM is close to an EOM;
(6) When a strong interaction occurs, if the FDCR of the EOM increases above 1, the ELCR of the EOM would drop below 1, which indicates that this EOM is no longer dominated by electromechanical dynamics, and thus is transformed into a quasi-EOM. The participation of FCWG may not only affect the system electromechanical dynamics, but also influence the FCWG dynamics; thus proper coordination of dynamic interaction is needed to avoid the negative effects;
(7) In the case of strong interaction, the integration of FCWG introduces a new quasi-EOM which relates to both system electromechanical dynamics and FCWG dynamics;
(8) The replacement of an SG with the FCWG significantly affects the system electromechanical dynamics. A local EOM may disappear in weak interaction cases, while new local quasi-EOMs may be introduced in strong interaction cases.

6. Conclusions

Due to the decoupling nature of FCWG, its dynamics can be normally neglected when studying the system electromechanical dynamics, whereas the exceptional case is a strong interaction between wind power generation and the grid. In this paper, we extensively investigated the participation of FCWG in the electromechanical dynamics of the power system and how it transforms the characteristics of the system's EOM. By using the mode identification criteria, the participation of FCWG in system electromechanical dynamics is quantified. It is found that in most scenarios when the FOMs have an oscillation frequency far from that of the EOMs, the participation of FCWG is quite limited, and the main impact of FCWG on the EOM is via the power flow injection. However, when an FOM has a similar frequency to that of an EOM, the participation of FCWG may become significantly active, or even dominate the EOM. In this condition, a transition from the traditional electromechanical dynamics to quasi-electromechanical dynamics was observed with the assistance of the proposed FDCR and QELCR.

Author Contributions: Completed the methodology, analysis, simulation, validation, and wrote the paper, J.L., supervised the research throughout, acquired funding, coordinated the project, and revised and edited the paper. S.B., reviewed and edited the paper, J.Z. All authors have read and agreed to the published version of the manuscript.

Funding: This research was funded by National Natural Science Foundation of China grant number (51807171), Guangdong Science and Technology Department grant number (2019A1515011226), Hong Kong Research Grant Council grant number (25203917), (15200418) and (15219619), and Department of Electrical Engineering, The Hong Kong Polytechnic University grant number (1-ZE68). The APC was funded by TPS Scheme of Hong Kong Polytechnic University.

Acknowledgments: The authors would like to acknowledge the support from the National Natural Science Foundation of China for the Research Project (51807171), the Guangdong Science and Technology Department for the Research Project (2019A1515011226), the Hong Kong Research Grant Council for the Research Projects (25203917), (15200418) and (15219619), the Department of Electrical Engineering, and the Hong Kong Polytechnic University for the Start-up Fund Research Project (1-ZE68).

Conflicts of Interest: The authors declare no conflict of interest.

References

1. Milano, F.; Dörfler, F.; Hug, G.; Hill, D.J.; Verbič, G. Foundations and Challenges of Low-Inertia Systems. In Proceedings of the 2018 Power Systems Computation Conference (PSCC), Dublin, Ireland, 11–15 June 2018; pp. 1–25.
2. Sun, J.; Li, M.; Zhang, Z.; Xu, T.; He, J.; Wang, H.; Li, G. Renewable Energy Transmission by HVDC across the Continent: System Challenges and Opportunities. *CSEE J. Power Energy Syst.* **2017**, *3*, 353–364. [CrossRef]
3. Hatziargyriou, N.; Milanović, J.; Rahmann, C.; Ajjarapu, V.; Cañizares, C.; Erlich, I.; Hill, D.; Hiskens, I.; Kamwa, I.; Pal, B. *Stability Definitions and Characterization of Dynamic Behavior in Systems with High Penetration of Power Electronic Interfaced Technologies*; IEEE PES Technical Report PES-TR77; IEEE Power and Energy Society (PES) Resource Center: Atlanta, GA, USA, 2020.
4. Li, Y.; Gu, Y.; Zhu, Y.; Ferre, A.J.; Xiang, X.; Green, T.C. Impedance Circuit Model of Grid-Forming Inverter: Visualizing Control Algorithms as Circuit Elements. *IEEE Trans. Power Electron.* **2020**, *36*, 3377–3395. [CrossRef]
5. Gu, Y.; Li, Y.; Zhu, Y.; Green, T. Impedance-Based Whole-System Modeling for a Composite Grid via Embedding of Frame Dynamics. *IEEE Trans. Power Syst.* **2020**. [CrossRef]
6. Gautam, D.; Goel, L.; Ayyanar, R.; Vittal, V.; Harbour, T. Control Strategy to Mitigate the Impact of Reduced Inertia Due to Doubly Fed Induction Generators on Large Power Systems. *IEEE Trans. Power Syst.* **2011**, *26*, 214–224. [CrossRef]
7. Hedayati-Mehdiabadi, M.; Zhang, J.; Hedman, K.W. Wind Power Dispatch Margin for Flexible Energy and Reserve Scheduling with Increased Wind Generation. *IEEE Trans. Sustain. Energy* **2015**, *6*, 1543–1552. [CrossRef]
8. Garmroodi, M.; Hill, D.J.; Verbic, G.; Ma, J. Impact of Tie-Line Power on Inter-Area Modes with Increased Penetration of Wind Power. *IEEE Trans. Power Syst.* **2016**, *31*, 3051–3059. [CrossRef]
9. Bialasiewicz, J.T.; Muljadi, E. The wind farm aggregation impact on power quality. In Proceedings of the IECON 2006-32nd Annual Conference on IEEE Industrial Electronics, Paris, France, 6–10 November 2006; pp. 4195–4200.
10. Knüppel, T.; Nielsen, J.N.; Jensen, K.H.; Dixon, A.; Østergaard, J. Power Oscillation Damping Capabilities of Wind Power Plant with Full Converter Wind Turbines Considering Its Distributed and Modular Characteristics. *IET Renew. Power Gener.* **2013**, *7*, 431–442. [CrossRef]
11. Knüppel, T.; Nielsen, J.N.; Jensen, K.H.; Dixon, A.; Ostergaard, J. Small-signal stability of wind power system with full-load converter interfaced wind turbines. *IET Renew. Power Gener.* **2012**, *6*, 79–91. [CrossRef]
12. Luo, J.; Bu, S.; Zhu, J.; Chung, C.Y. Modal Shift Evaluation and Optimization for Resonance Mechanism Investigation and Mitigation of Power Systems Integrated with FCWG. *IEEE Trans. Power Syst.* **2020**, *35*, 4046–4055. [CrossRef]
13. Du, W.; Chen, X.; Wang, H. PLL-Induced Modal Resonance of Grid-Connected PMSGs with the Power System Electromechanical Oscillation Modes. *IEEE Trans. Sustain. Energy* **2017**, *8*, 1581–1591. [CrossRef]
14. Ying, J.; Yuan, X.; Hu, J.; He, W. Impact of Inertia Control of DFIG-Based WT on Electromechanical Oscillation Damping of SG. *IEEE Trans. Power Syst.* **2018**, *33*, 3450–3459. [CrossRef]
15. Sun, L.; Liu, K.; Hu, J.; Hou, Y. Analysis and Mitigation of Electromechanical Oscillations for DFIG Wind Turbines Involved in Fast Frequency Response. *IEEE Trans. Power Syst.* **2019**, *34*, 4547–4556. [CrossRef]
16. Singh, M.; Allen, A.J.; Muljadi, E.; Gevorgian, V.; Zhang, Y.; Santoso, S. Interarea Oscillation Damping Controls for Wind Power Plants. *IEEE Trans. Sustain. Energy* **2015**, *6*, 967–975. [CrossRef]
17. Silva-Saravia, H.; Pulgar-Painemal, H. Effect of Wind Farm Spatial Correlation on Oscillation Damping in the WECC System. In Proceedings of the 2019 North American Power Symposium (NAPS), Wichita, KS, USA, 13–15 October 2019; pp. 1–6.

18. Mokhtari, M.; Aminifar, F. Toward Wide-Area Oscillation Control through Doubly-Fed Induction Generator Wind Farms. *IEEE Trans. Power Syst.* **2014**, *29*, 2985–2992. [CrossRef]
19. Liao, K.; He, Z.; Xu, Y.; Chen, G.; Dong, Z.Y.; Wong, K.P. A Sliding Mode Based Damping Control of DFIG for Interarea Power Oscillations. *IEEE Trans. Sustain. Energy* **2017**, *8*, 258–267. [CrossRef]
20. Boubzizi, S.; Abid, H.; Chaabane, M. Comparative study of three types of controllers for DFIG in wind energy conversion system. *Prot. Control Mod. Power Syst.* **2018**, *3*, 21. [CrossRef]
21. Gurung, N.; Bhattarai, R.; Kamalasadan, S. Optimal Oscillation Damping Controller Design for Large-Scale Wind Integrated Power Grid. *IEEE Trans. Ind. Appl.* **2020**, *56*, 4225–4235. [CrossRef]
22. Morató, J.; Knüppel, T.; Østergaard, J. Residue-Based Evaluation of the Use of Wind Power Plants with Full Converter Wind Turbines for Power Oscillation Damping Control. *IEEE Trans. Sustain. Energy* **2014**, *5*, 82–89. [CrossRef]
23. Fan, L.; Yin, H.; Miao, Z. On Active/Reactive Power Modulation of DFIG-Based Wind Generation for Interarea Oscillation Damping. *IEEE Trans. Energy Convers.* **2011**, *26*, 513–521. [CrossRef]
24. Elhaji, E.M.; Hatziadoniu, C.J. Damping tie line oscillation using permanent magnet wind generators in the Libyan power system. In Proceedings of the 2014 North American Power Symposium (NAPS), Pullman, WA, USA, 7–9 September 2014; pp. 1–6.
25. Bu, S.; Du, W.; Wang, H. Model validation of DFIGs for power system oscillation stability analysis. *IET Renew. Power Gener.* **2017**, *11*, 858–866. [CrossRef]
26. Bu, S.Q.; Zhang, X.; Zhu, J.B.; Liu, X. Comparison analysis on damping mechanisms of power systems with induction generator based wind power generation. *Int. J. Electr. Power Energy Syst.* **2018**, *97*, 250–261. [CrossRef]
27. Xia, S.W.; Bu, S.Q.; Zhang, X.; Xu, Y.; Zhou, B.; Zhu, J.B. Model reduction strategy of doubly-fed induction generator-based wind farms for power system small-signal rotor angle stability analysis. *Appl. Energy* **2018**, *222*, 608–620. [CrossRef]
28. Jafarian, M.; Ranjbar, A.M. Interaction of the dynamics of doubly fed wind generators with power system electromechanical oscillations. *IET Renew. Power Gener.* **2013**, *7*, 89–97. [CrossRef]
29. Ge, Y.; Cai, H.; Cao, J.; Wang, H.F. Impact of large scale wind power penetration on power system oscillations based on electric torque analysis. In Proceedings of the International Conference on Sustainable Power Generation and Supply, Hangzhou, China, 8–9 September 2012; pp. 1–7.
30. Luo, J.; Bu, S.; Teng, F. An Optimal Modal Coordination Strategy based on Modal Superposition Theory to Mitigate Low Frequency Oscillation in FCWG Penetrated Power Systems. *Int. J. Electr. Power Energy Syst.* **2020**, *120*, 105975. [CrossRef]
31. Wilches-Bernal, F.; Chow, J.H.; Sanchez-Gasca, J.J. Impact of wind generation power electronic interface on power system inter-area oscillations. In Proceedings of the IEEE Power and Energy Society General Meeting (PESGM), Boston, MA, USA, 17–21 July 2016; pp. 1–5.
32. Luo, J.; Bu, S.; Zhu, J. A Novel PMU-based Adaptive Coordination Strategy to Mitigate Modal Resonance between Full Converter-based Wind Generation and Grids. *IEEE J. Emerg. Sel. Top. Power Electron.* **2020**. [CrossRef]
33. Du, W.; Bi, J.; Wang, H. Damping Degradation of Power System Low-Frequency Electromechanical Oscillations Caused by Open-Loop Modal Resonance. *IEEE Trans. Power Syst.* **2018**, *33*, 5072–5081. [CrossRef]
34. Kundur, P.; Balu, N.J.; Lauby, M.G. *Power System Stability and Control*; McGraw-Hill: New York, NY, USA, 1994; Volume 7.
35. Wang, X.-F.; Song, Y.; Irving, M. *Modern Power Systems Analysis*; Springer Science & Business Media: New York, NY, USA, 2010.